JMEPEG (1994): 712-721

Finite Element Modeling of Segmental Chip Formation in High-Speed Orthogonal Cutting

J. Hashemi, A.A. Tseng, and P.C. Chou

An explicit, Lagrangian, elastic-plastic, finite element code has been modified to accommodate chip separation, segmentation, and interaction in modeling of continuous and segmented chip formation in high-speed orthogonal metal cutting process. A fracture algorithm has been implemented that simulates the separation of the chip from the workpiece and the simultaneous breakage of the chip into multiple segments. The path of chip separation and breakage is not assigned in advance but rather is controlled by the state of stress and strain induced by tool penetration. A special contact algorithm has been developed that automatically updates newly created surfaces as a result of chip separation and breakage and flags them as contact surfaces. This allows for simulation of contact between tool and newly created surfaces as well as contact between simulated chip segments. The work material is modeled as elastic/perfectly plastic, and the entire cutting process from initial tool workpiece contact to final separation of chip from workpiece is simulated. In this paper, the results of the numerical simulation of continuous and segmented chip formation in orthogonal metal cutting of material are presented in the form of chip geometry, stress, and strain contours in the critical regions.

Keywords

chip formation, finite element, fracture algorithm, modeling, orthogonal cutting

1. Introduction

NEARLY every component in use in our society has undergone the machining process at some stage within its manufacturing cycle. As a result, the economics of the machining process plays an important role in the manufacturing costs of countries such as United States. There are several reasons for developing a rational approach to material removal, such as improving cutting techniques, producing products with enhanced precision, and increasing the rate of production (Ref 1). The economics of the cutting process has made this area one of paramount importance from both the technical and the engineering economics points of view.

Attempts to understand the mechanics of the metal cutting process date back to the work performed by Cocquilhat in 1851, when he measured the work required to remove a portion of material by drilling. Other early investigations in the general area of metal cutting were performed by Time (Ref 2) and Treska (Ref 3), in which calculations for determining the resistance of metals to cutting were documented. A systematic scientific study of the art of metal cutting started when Taylor (Ref 4) studied the economics of metal machining. Since the mid-1930s, there have been numerous attempts to develop a relatively simple model of the cutting process. Examples of such studies are those performed by Piispanen (Ref 5) and that of Ernst and Merchant (Ref 6). Piispanen tried to predict the shear angle for a wide range of cutting conditions, but his work, which was a graphical analysis, did not lead to any analytical expressions. Ernst and Merchant, however, presented the first qualitative analysis of the process and developed a model relating the shear angle to friction and rake angle. Lee and Schaffer (Ref 7) took an analytical approach to the problem and produced a new shear zone solution through the application of slip line field theory. Many other shear zone solutions have appeared in the literature and have included important material factors such as work hardening, strain rate hardening, and temperature effects. However, none of the proposed models has generated satisfactory results. This could be due to simplifying and restrictive assumptions that were made.

With the introduction of finite element techniques, many attempts have been made to model the metal cutting process through utilization of this method. One of the important goals has been to model the formation of the chip as the material is removed from the surface of the workpiece and to determine the subsequent state of deformation in the workpiece as well as in the chip material. Klamecki's work (Ref 8) is the first example of such effort. Klamecki used a three-dimensional formulation to treat the incipient chip formation process. Usui and Shirakashi (Ref 9) developed a model based on empirical data for rate-independent behavior. The model was suitable for steady-state cutting conditions. Iwata, Osakada, and Terasaka (Ref 10) simulated a low-speed metal cutting process based on a rigid-plastic constitutive law. The residual stresses could not be determined due to the rigid-plastic deformation behavior.

Thus far, the most realistic simulations (all plane strain simulations) have been performed by Strenkowski and Carrol (Ref 11), Carrol and Strenkowski (Ref 12), and most recently, Komvopoulos and Erpenbeck (Ref 13). Strenkowski and Carrol used the Lagrangian NIKE2D code to model the orthogonal metal cutting process. They simulated the formation of a continuous chip in the steady-state condition and calculated the state of residual stresses according to a temperature-dependent

J. Hashemi, Department of Mechanical Engineering, Texas Tech University, Lubbock, TX 79409; and **A.A. Tseng** and **P.C. Chou,** Department of Mechanical Engineering and Mechanics, Drexel University, Philadelphia, PA 19104.

constitutive model and adiabatic conditions. Severe distortion of the mesh due to large deformation presented some difficulties by reducing the integration time increment. This is a problem associated with all Lagrangian codes used to simulate large deformation problems where computationally expensive remeshing techniques must be used. It should be mentioned that a predetermined chip separation path was utilized in Strenkowski and Carrol's numerical scheme; that is, whenever the tool reached the critical node on the separation path, according to the state of plastic strain surrounding the node, the node would split from the surface. The initial geometry of the chip material was distorted. This modification was made to avoid simulation complications as a result of high compressive deformations around the tool-workpiece interface.

Carrol and Strenkowski used an identical procedure and a similar constitutive equation while taking into account the effect of strain rate. Most recently, Komvopoulos and Erpenbeck utilized the finite element method to model chip formation in orthogonal metal cutting. To simulate separation of the chip from the workpiece, two nodes were superimposed at each nodal location of a prearranged parting line of the initial mesh. Simply stated, the nodes on the parting line separated when the tool tip was in close, predetermined proximity to that node. Constitutive equations of elastic/perfectly plastic and elastic-plastic with strain rate sensitivity were used in different simulations. Tool material and builtup edge were modeled as rigid. The simulation was based on the assumption that the chip had already partially formed. The reason for that assumption, according to the authors, was to reduce the computation time. The actual simulation shape of the chip material was determined based on experimental results. The authors stated that fair agreement between experimental and numerical results was observed. It should be mentioned that their simulation included effects of friction on the chip-tool contact interface as well as tool wear at the rake face.

The above-mentioned studies have all been related to cases where continuous chips are formed, and the objective has been to gain a qualitative insight into some specific aspects of the machining process. The modeling of the machining process where segmental chips are formed has not appeared in the literature.

In addition, most studies do not utilize a systematic approach in modeling the complete process from the initial tool work contact through chip formation and separation. For example, in some modeling attempts, the geometry of the chip has been input to the code, and the simulation has been performed based on an existing chip. Another shortcoming in recent machining simulations has been the unavailability of an algorithm capable of simulating dynamic metal fracture, without the use of a predetermined chip separation path, as the tool penetrates the workpiece. This is especially important when simulating segmental chip formation, which requires an algorithm that can handle element separation, new node creation, element reattachment, and finally sliding surface insertion and modification. Sliding-surface insertion and modification is required to simulate the contact between opposite surfaces of a crack as they interact. This paper presents the theoretical formulation, related algorithms, and simulation results of a finite element scheme capable of simulating segmental chip formation.

2. Numerical Scheme

A two-dimensional Lagrangian finite element computer program, originally developed for dynamic analysis of impact and explosive-metal interaction problems, has been modified to simulate the chip formation process. The program uses the Lagrangian finite element formulation, where the equations of motion of each mass node are integrated directly and explicitly. An important feature of the program is that unlike the conventional finite element modeling programs, the global stiffness matrix is not used; instead, the nodal forces are directly calculated from the element stresses at each time step during the integration. The program includes multiple sliding surfaces between elements, which is most suitable in treating the interface condition. Triangular elements are utilized in the code due to their suitability in problems with severe deformation.

The formulation of the code is based on the hydrocode approach, similar to that used by Chou and Wu (Ref 14) and Chou et al. (Ref 15). The first step in the program is to represent the geometry by triangular elements and lump the mass at the nodes (element corners). Initial velocities are assigned to those nodes where the movement is prescribed. If any external forces are applied on part of the boundary, they are concentrated on the corresponding nodes and superimposed on the nodal forces due to stresses in the adjacent elements. The displacement fields in each element are assumed to be linear functions of space and are expressed in terms of nodal displacements. The velocity fields and the strain rates in the element are then calculated from the nodal velocities. Stresses are calculated based on increments of strains and the constitutive relations. The detailed equations about the calculation of the strains and the strain rates are presented by Chou and Wu (Ref 14). The remainder of this section will focus on the calculation of stresses from the strain rate at the previous time step.

In hydrocodes, where the pressure involved is very high, the material cannot be simply considered elastic-plastic. Material must be treated as a compressible material, and an equation of state relating the pressure, density, and internal energy must be used in place of the elastic spherical stress-strain relation. To facilitate this, the plastic constitutive equations are expressed in terms of deviatoric stress and strain. Another point is that the numerical procedure involves the calculation of stress from the total strain rate, not the plastic strain rate, at each time increment cycle. Therefore, a constitutive relation of stress in terms of total strain rate is needed.

Considering the "associated plasticity," where the yield function and plastic potential are identical, the plastic strain increment can be expressed as:

$$d\varepsilon_p = \lambda \frac{\partial f}{\partial \sigma} \qquad \text{(Eq 1)}$$

where ε_p is the plastic strain, f is the plastic potential, $f(\sigma, k) = 0$ is the yield criterion, σ is the stress, k is the hardening parameter, and λ is defined below. The total strain increment can be divided into elastic and plastic parts:

$$d\varepsilon = d\varepsilon_e + d\varepsilon_p = \mathbf{D}^{-1} d\sigma + \lambda \frac{\partial f}{\partial \sigma} \quad \text{(Eq 2)}$$

where ε is the effective strain, ε_e is the elastic strain, and $\mathbf{D}$ is the elasticity matrix. This equation can be inverted to give the stress increment in terms of the total strain increment:

$$d\sigma = \mathbf{D} d\varepsilon - \lambda \mathbf{D} \frac{\partial f}{\partial \sigma} \quad \text{(Eq 3)}$$

where

$$\lambda = \left\{\frac{\partial f}{\partial \sigma}\right\}^T \mathbf{D} \{d\varepsilon\} \left[\left\{\frac{\partial f}{\partial \sigma}\right\}^T \mathbf{D} \left\{\frac{\partial f}{\partial \sigma}\right\} + A\right]^{-1} \quad \text{(Eq 4)}$$

and

$$A = \frac{-\partial f}{\partial k} \{\sigma\}^T \frac{\partial f}{\partial \sigma} \quad \text{(Eq 5)}$$

For isotropic or orthotropic flow rules, such as von Mises' or Hill's, where the normal stresses and shear stresses are not coupled in the yield criterion, it can be shown that

$$\frac{\partial f}{\partial \sigma} = \frac{\partial f}{\partial s} \quad \text{(Eq 6)}$$

where s is the stress deviator. The stress deviator increment, ds, can be given as:

$$ds = \mathbf{D} de - \lambda \mathbf{D} \frac{\partial f}{\partial s} \quad \text{(Eq 7)}$$

where

$$\lambda = \left\{\frac{\partial f}{\partial s}\right\}^T \mathbf{D} \{de\} \left[\left\{\frac{\partial f}{\partial s}\right\}^T \mathbf{D} \left\{\frac{\partial f}{\partial s}\right\} + A\right]^{-1} \quad \text{(Eq 8)}$$

$$de = d\varepsilon - \mathbf{D}^{-1} d\sigma_m, A = \frac{-\partial f}{\partial k} \{s\}^T \frac{\partial f}{\partial s} \quad \text{(Eq 9)}$$

and e is the strain deviator and σ_m is the mean stress.

In the numerical calculations, at time t the deviator stress and strain rate components are known. The stress deviator at the next time step, $s_{i.tr_1}^{t+\Delta t}$, is determined by first calculating a trial stress based on elastic stress deviator increment:

$$s_{i.tr_1}^{t+\Delta t} = s_i + 2G\dot{e}_i \Delta t + \omega_i \Delta t \quad i = 1, 2, \ldots 6 \quad \text{(Eq 10)}$$

where $\dot{e}$ is the strain rate deviator, G is the shear modulus, and the subscript i = 1, 2, 3 for the three normal components and 4, 5, 6 for the three shear components. Note that the tensorial shear strains are used. The ω_i term represents the contribution due to element rotation. With $\omega_{\theta z} = \omega_{\theta r} = 0$, it can be shown that

$$\begin{aligned} \omega_1 &= -2\sigma_4 \omega_{rz} \\ \omega_2 &= 2\sigma_4 \omega_{rz} \\ \omega_4 &= (\sigma_1 - \sigma_2)\omega_{rz} \\ \omega_3 &= \omega_5 = \omega_6 = 0 \end{aligned} \quad \text{(Eq 11)}$$

For the von Mises yield condition, we shall use the equivalent stress, $\bar{\sigma}$:

$$\bar{\sigma} = \left[\frac{3}{2}\left(s_1^2 + s_2^2 + s_3^2\right) + 3\left(s_4^2 + s_5^2 + s_6^2\right)\right]^{1/2} \quad \text{(Eq 12)}$$

If $\bar{\sigma} < \sigma_y$ (the effective flow stress), the material is elastic, and the trial stress is the correct stress at time $t + \Delta t$. If $\sigma > \sigma_y$, the material has yielded and a second trial stress is calculated:

$$s_{i.tr_2}^{t+\Delta t} = s_i + 2G\dot{e}_i \Delta t - 2G(1 - \alpha)\lambda s_i + \omega_i \Delta t \quad i = 1, 2, \ldots, 6 \quad \text{(Eq 13)}$$

where α is the percent of the stress increment inside the yield surface.

The stress deviator increment in this trial stress deviator, not counting the rotational term, is:

$$\Delta s_i = 2G\dot{e}_i \Delta t - 2G\lambda s_i \quad \text{(Eq 14)}$$

This is exactly the Prandtl-Reuss flow rule:

$$de_i = \frac{1}{2G} ds_i + \lambda s_i \quad \text{(Eq 15)}$$

Therefore, in using the trial stress in Eq 13, we satisfied the von Mises yield condition and the Prandtl-Reuss flow rule. However, due to the finite increment in time, Δt, the resulting state of stress, even though following a path tangent to the yield surface, may still fall outside of it. To correct this, the final stress deviator at $t + \Delta t$ is obtained from $s_{i.tr_2}$ by:

$$s_i^{t+\Delta t} = s_{i.tr_2} \frac{\sigma_y}{\bar{\sigma}_{tr_2}} \quad \text{(Eq 16)}$$

where $\bar{\sigma}_{tr_2}$ is the equivalent stress calculated from $s_{i.tr_2}^{t+\Delta t}$.

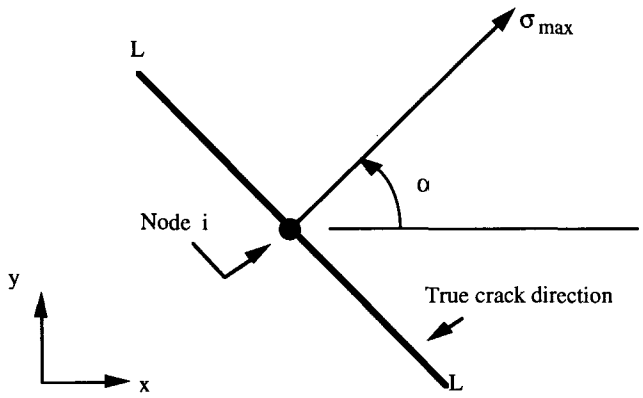

Fig. 1 Determination of the true crack direction

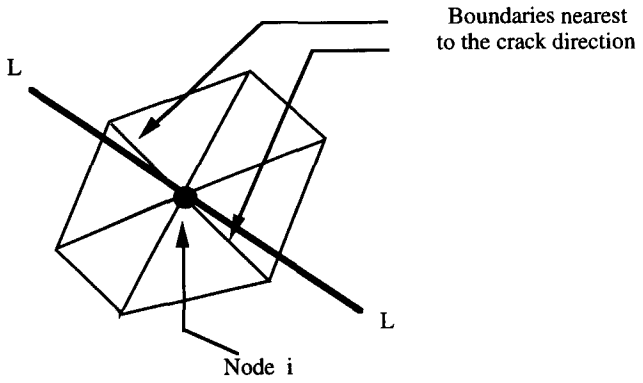

Fig. 2 Determination of the boundaries nearest to the crack direction

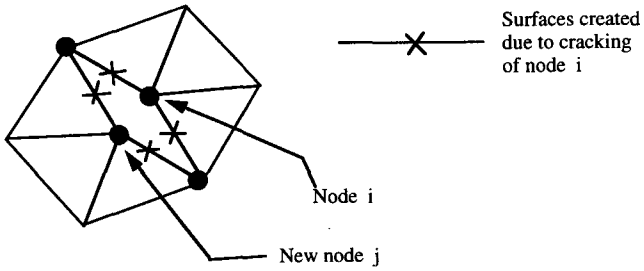

Fig. 3 Crack initiation and splitting of the node

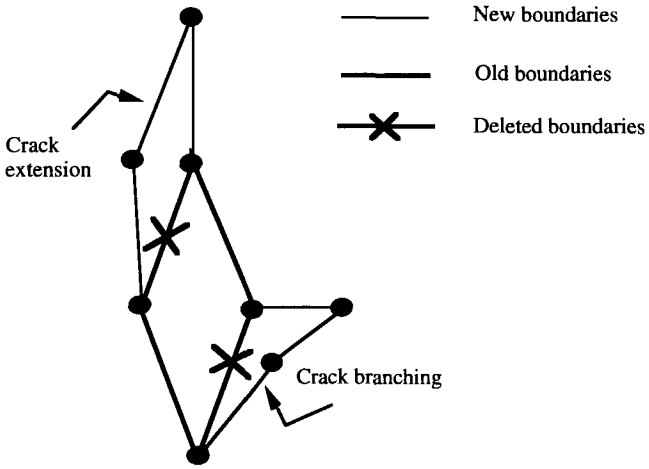

Fig. 4 Crack branching, extension and formation of new boundaries

3. Sliding-Surface Algorithm

A new algorithm has been adopted to simulate segmented chip formation. The fracture element routine and a new sliding-surface algorithm have been created for this purpose. The following is a description of the above algorithm and the fracture element developed. The new algorithm makes the code capable of simulating the following cases: crack initiation, based on a proper fracture criterion; crack extension, branching and joining; and dynamic insertion of sliding-surfaces where cracks were initiated, in order to simulate the contact between the opposite surfaces of cracks and the tool workpiece.

The fracture element routine begins, in each computational cycle, by evaluating the maximum normal stress (principal stress) at each node. Each tensorial component of stress, an element property, is found at a node by averaging the stresses in the attached elements. In cases where a sharp stress gradient exists, the routine analyzes the elements attached to the node separately and records the maximum value of the principal stress in those elements. If the magnitude of the principal stress exceeds a critical value, taken as the material fracture strength, a crack is assumed to initiate along a direction normal to the stress vector (Fig. 1).

The algorithm then searches for the two element boundaries at the node that run nearest to the intended crack direction (Fig. 2). Once the boundaries are determined, the single node under consideration splits. The splitting action is simulated by adding a new node at the point of splitting and then reattaching the proper elements across the crack to the proper nodes.

The mass of the original node is divided between the two new nodes in proportion to the number of elements attached to each; positions and velocities of the new nodes are taken as those of the old node. Finally, a sliding interface is defined across the crack. The material on opposite sides of the crack may thus separate or slide (with or without friction) relative to each other, but may not cross (Fig. 3).

Special routines treat propagation and interaction of cracks (Fig. 4). Extension of a crack involves repeated splitting of the end node and insertion of new sliding-surfaces in the direction of extension, and/or deletion of some old ones. On branching of a crack, a previously splitted node splits again, and sliding-surfaces are inserted at the branching point. Each subsequent splitting action is assumed to be governed by the same fracture criterion that governs the first initiated crack.

The simulation of the segmented chip formation required the development of a new sliding-surface algorithm significantly different from conventional ones. The drawback with the conventional sliding-surface algorithms is that the contact

interfaces have to be defined in terms of the nodes constructing them, in a continuous manner and with the specific numbering sequence, as discussed by Hashemi (Ref 16). This restriction often causes great difficulty in automatic creation of fracture lines. Every time a new surface is introduced to the geometry, all the existing sliding surfaces have to be modified and new node numbers have to be inserted in the proper position in the sliding-surface. The updating task requires extensive programming and is extremely expensive from a computational point of view. The sliding-surface algorithm in this code has been restructured to simulate the contact surface between the tool and the workpiece as well as to create and simulate the interaction between chip segments.

The sliding-surface algorithm is activated by the main program in each computational cycle. Initially, a series of nodes lying on the surface are located and labeled as boundary nodes. In the method employed here, a set of nodal points that define element edges on the surface of the material define unique boundary segments on which other boundary nodes are not permitted to intrude. These boundary segments are not required to define the material surface in a continuous manner. The major advantage of the new formulation is that the interacting boundaries are defined by a series of boundary segments, as opposed to a continuous series of nodes. If a crack develops, the whole sliding surface need not be modified. Only the new segments have to be added to the boundary segment array. When a boundary node penetrates a boundary segment, the intrusion is cleared by updating the location of the intruding node. The new location of the node is determined by projecting the coordinates of the node perpendicular to and along the intruded segment. The readjustment of the coordinates of the node are accompanied by applying the principle of conservation of linear momentum between the node and the segment. The unique characteristic of this routine is that the boundary nodes of one body will be checked against the boundary segments of the same body and therefore avoid the folding of the surface of the same body on itself. This simulates the contact between newly created surfaces or fractured surfaces.

Each temporal integration increment is comprised of the following steps:

1. Determine the boundary nodes and the boundary segments of all the bodies included in the simulation.
2. For every boundary node, check all the boundary segments of all the bodies that encompass the boundary node. Determine if penetration of the segment has occurred, using the following steps.
3. Find the intersection point between the boundary segment and the boundary node vector that traces the path of the boundary node from one cycle to the next.
4. If the intersection is within the bounds of both vectors, penetration is confirmed. Proceed with step 5.
5. Determine whether the final position of the boundary node is within the bounds of the segment. If yes, proceed with step 6; otherwise, proceed with step 7.
6. Project the intruding boundary node perpendicular to the boundary segment. Update its position and its velocities by conserving the angular momentum between the node and the segment. Repeat the procedure for the next node in the array.
7. In the case where the final position of the boundary node is not within the segment under consideration, search for penetration in one of the adjacent boundary segments.

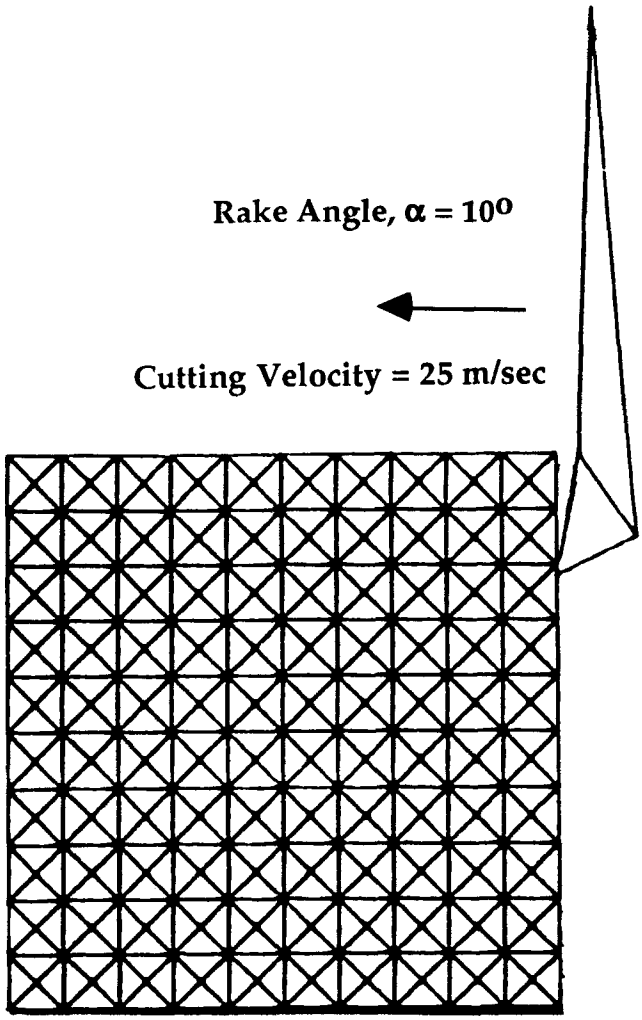

Fig. 5 Initial geometry of the orthogonal cutting process, plane strain simulation

4. Metal Cutting Simulation Results and Discussion

The above code was applied in simulation of high-speed machining of materials with the goal of simulating segmental chips. A plane strain simulation of orthogonal metal cutting processes at high cutting speeds was performed. Figure 5 shows the initial geometry of the simulation in which a cutting speed of 25 m/s and a rake angle of 10° were used. All surfaces were simulated as frictionless, and the cutting tool was modeled as rigid. A coarse finite element mesh was utilized to mini-

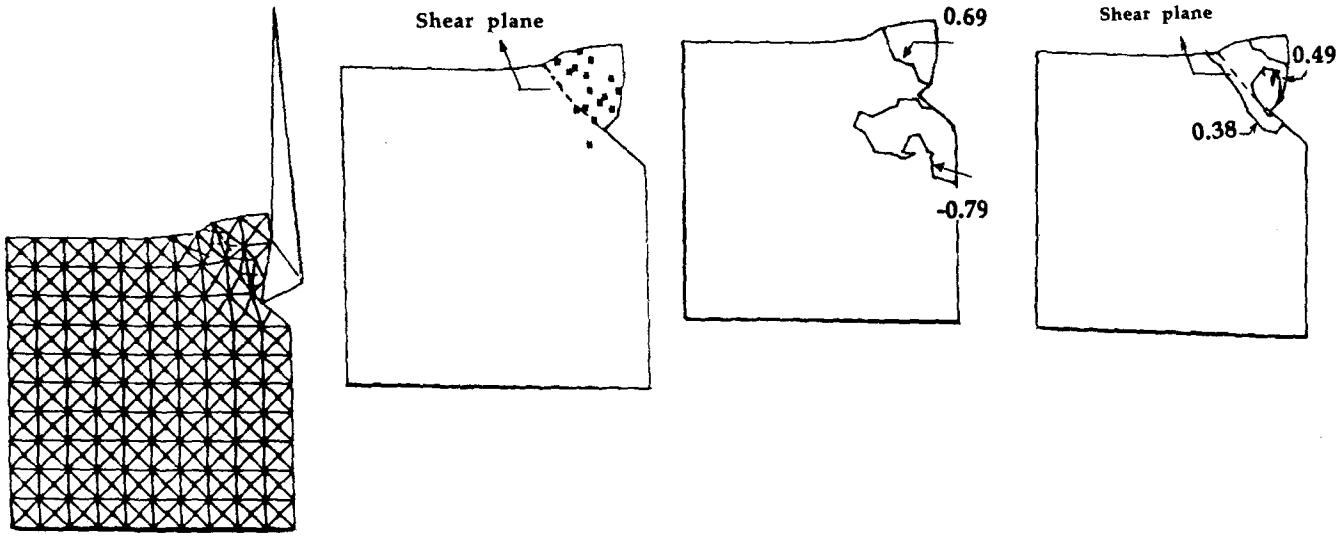

Fig. 6 Chip compression and separation stage. (a) Mesh geometry. (b) Plastic zone. (c) Shear stress distribution. (d) Effective plastic strain distribution

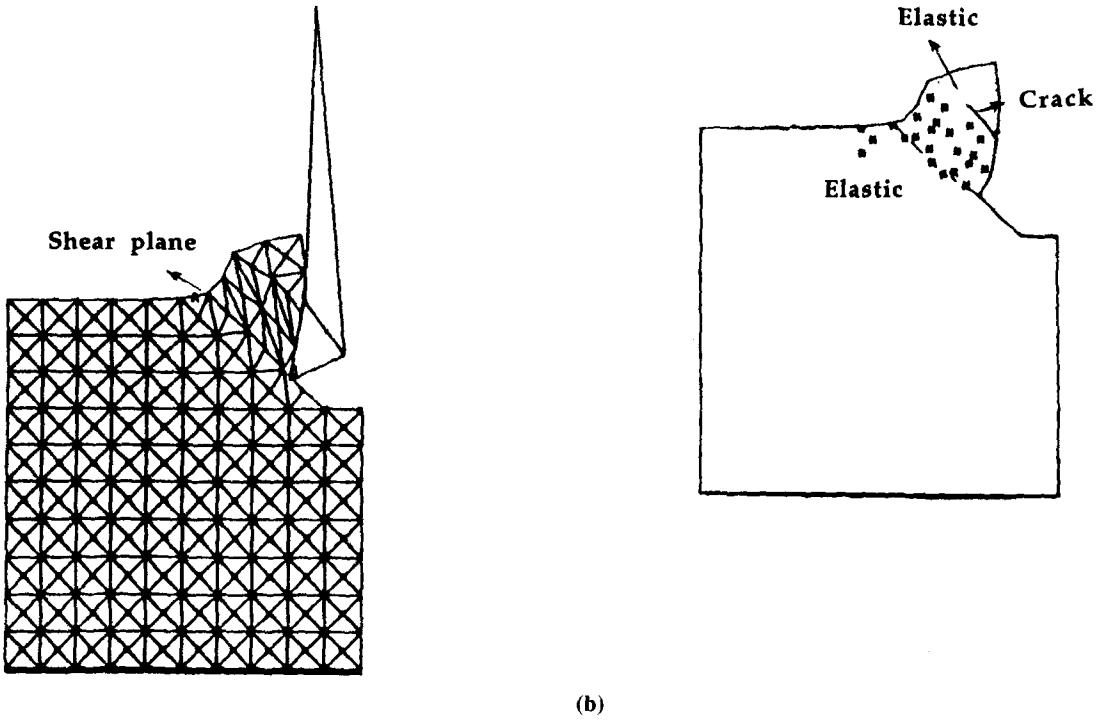

Fig. 7 Development of the primary and secondary shear zones. (a) Mesh geometry. (b) Plastic zone and formation of crack in the chip material

mize computational expense; however, for more accurate and realistic simulations a finer mesh has to be utilized. An elastic/perfectly plastic material constitutive equation was used to simulate the workpiece material. No attempts were made to model a specific material; however, the material constants used were those of an aluminum alloy: shear modulus 27.6 GPa, yield strength 517 MPa, and bulk modulus 76.6 GPa. The simulation was primarily intended to provide numerical capability to model continuous and segmented chip formation in high-speed machining of metals. Fracture elements together with the sliding surface algorithm were implemented to achieve the simulation objectives. Cracks initiated at nodal points where

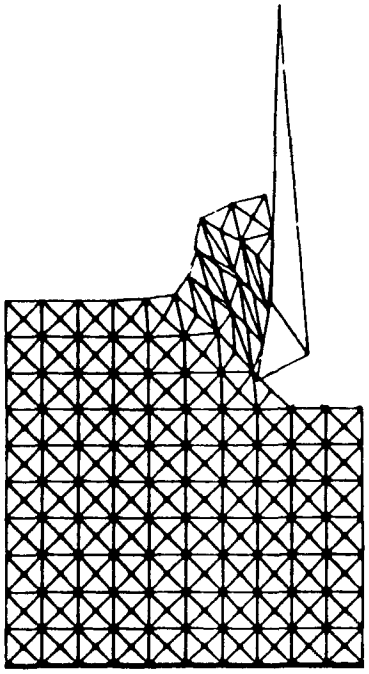

(a)

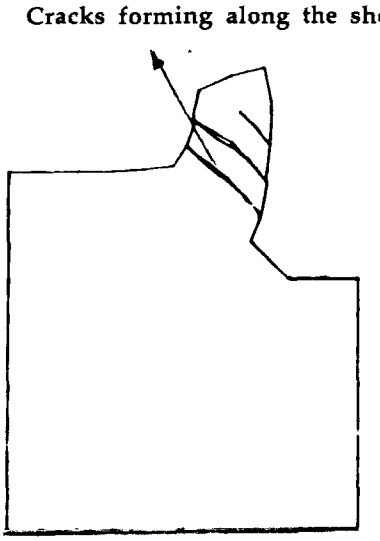

(b)

Fig. 8 Clear segmentation of the chip. (a) Mesh geometry. (b) Outline plot showing the formation of the cracks along the shear plane

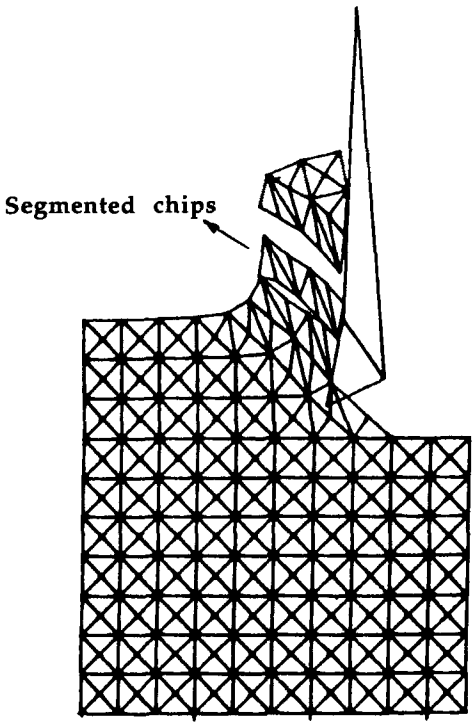

(a)

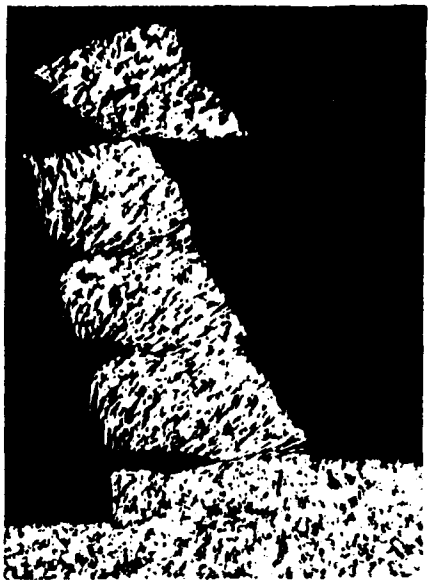

(b)

Fig. 9 Comparison of finite element simulation and experimental observation of the chip formation process. (a) Code results. (b) Experimental results

the fracture criterion was exceeded, extending in a direction normal to the principal stress direction at that point. The fracture criterion used for this simulation was based on the ultimate plastic strain of the material.

In the first trial, the geometry, boundary conditions, and cutting parameters were those outlined above. A fracture criterion based on effective plastic strain was used with a critical value of 0.6. A failure criterion was added in order to fail material that would deform excessively. Any element that experienced an effective plastic strain of 0.9 was failed. The failure action creates a series of failed and partially failed elements that are automatically fropped out of the computation cycle and are no longer part of the work material. Figures 6 through 10 show the results

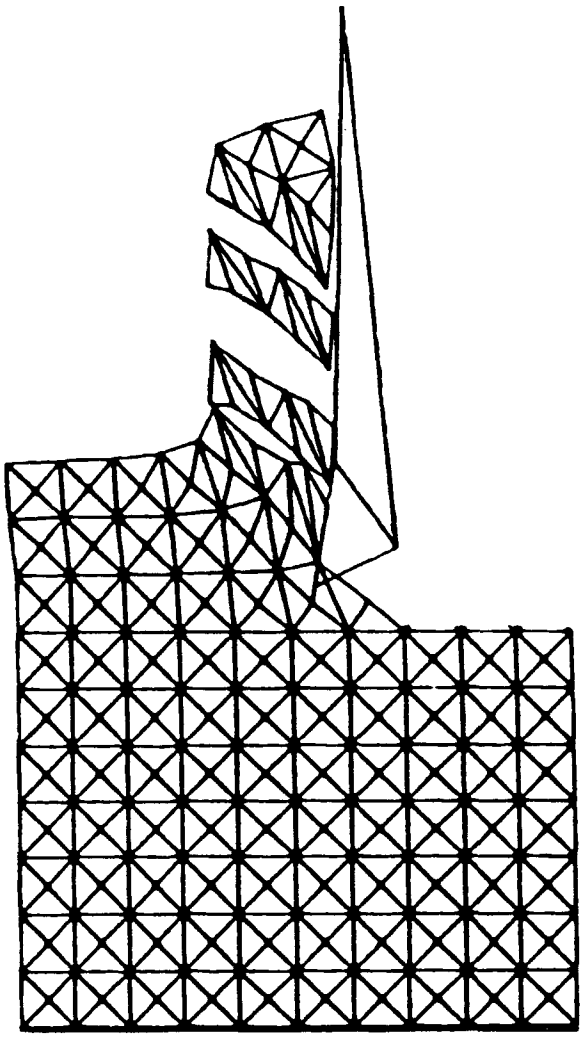

Fig. 10 Quasistatic stage of segmented chip formation

produced in the first trial. Figure 6(a) shows the initiation of the chipping process and the formation of a shear zone that starts from the tool tip and ends at the free surface. Figure 6(b) shows the plastic region around the tool tip at the corresponding computational cycle. The plastic region approximately represents the shear plane. This figure shows the outline of the workpiece but does not show formation of any cracks in the chip material. The shearing stress contour of the segmented chip simulations, at the stage corresponding, is presented in Fig. 6(c). It shows that the areas of high shear are located at the upper portion of the chip, where the shear stress is positive, and just below the tool, where the shear stress is maximum and negative. The high shear values in the chip material coincide with the approximate location of the shear plane. Figure 6(d) shows the distribution of the effective plastic strain. The three contours with the highest values are drawn, and it is shown that the contour of plastic strain is consistent with the location of the shear zone. The same approximate distribution of effective plastic strain exists at the later computational cycles.

The first evidence of chip segmentation is observed in Fig. 7(a), where the extensive shearing action on the chip material is obvious. The segmentation of the chip is clearly shown in Fig. 7(b), in which a crack is initiated from the inner chip surface. A comparison of Fig. 7(a) and (b) supports the observations made in the literature that the material undergoes plastic deformation in the shear zone and becomes elastic upon exiting the shear zone. Figure 8(a) shows the clear segmentation of the chip material along the shear plane, while Fig. 8(b) represents the outline of the workpiece and the corresponding cracks. It is important to note that the contact between opposite sides of the cracks is simulated adequately and that no interpenetration of materials is observed.

Figures 9(a) and 10 represent two later stages of the cutting process, where the segmented chips are continuously forming and moving away from the cutting tool at speeds higher than the cutting speed. The results are in good qualitative agreement with those cases where the chip material breaks due to brittle fracture. Figures 9(a) and (b) show the numerical simulation and experimental observation of the segmented chips. The simulated chip geometry is similar to that produced in the experiments (Ref 17).

A second trial was prepared with the same geometry and cutting conditions; however, a failure criterion of 1.5 was used to simulate continuous chip machining. Figure 11 shows the cutting geometry at different stages of the process. Figure 11(b) shows the formation of a shear zone where the deformation is considerably higher than at other regions of the workpiece. Separation of the chip from the tool surface is evident in Fig. 11(c), and it can also be observed that the chip thickness is in general greater than the depth of cut, which is consistent with experimental observations. The comparison of experimental results of continuous chip formation (Ref 17) with the numerical simulation is presented in Fig. 12. Figures 13(a) to (c) present the results in determining the distribution of effective plastic strain at different stages. These results show high values of plastic strain at the chip along the tool face. The general chip shape also agrees with the results given by Strenkowski and others.

5. Summary and Conclusions

The objective of this paper is to present the capability of a recently developed finite element scheme to assist in modeling of the orthogonal metal cutting process with both continuous and segmental chip formation. A dynamic finite element analysis of the orthogonal metal cutting process was performed. A fracture algorithm was developed that automatically generated splitting of the elemental nodes as the cutting tool penetrated the workpiece. The splitting of the node was dependent on the state of strain of the elements attached to it, while the corresponding direction of the crack was determined by a direction perpendicular to the average principal stresses at that node. In order to account for the contact between opposite sides of the crack, and in general all segments and bodies coming in contact, an automatic sliding-surface generation algorithm was developed. The modified code was utilized in simulation of orthogonal metal cutting with the objective of simulating continuous chip formation as well as segmental chip formation due

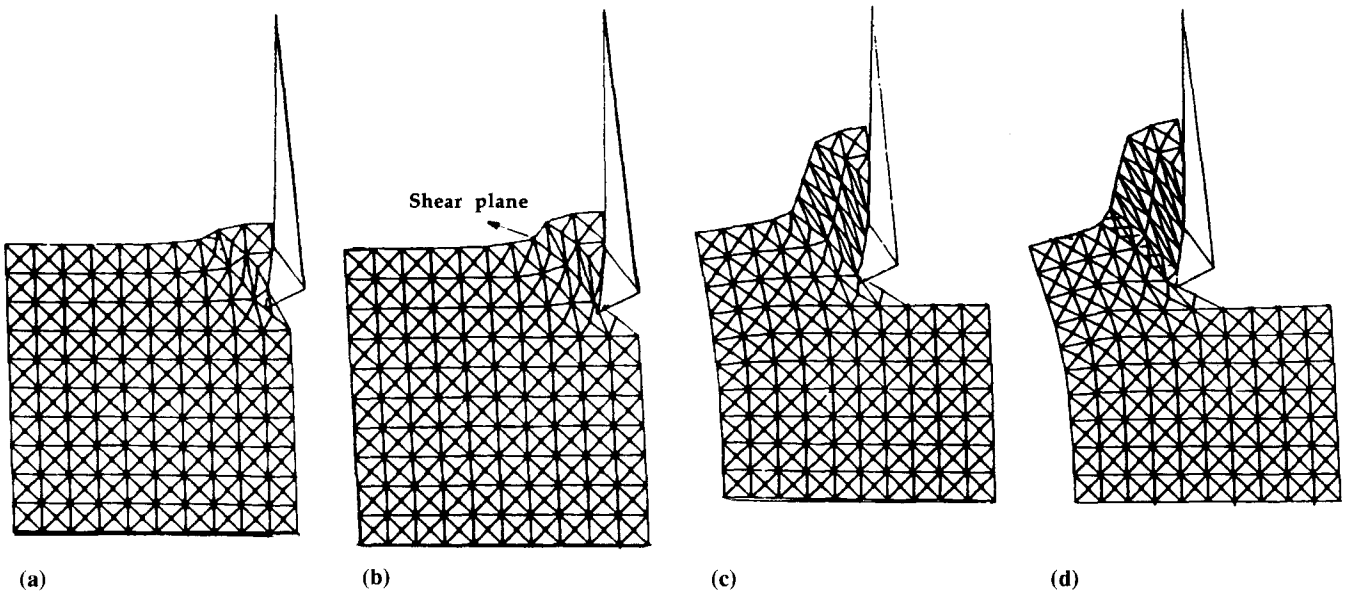

Fig. 11 Different stages of the cutting process associated with continuous chip formation. (a) Initial compression of the chip material. (b) Formation of the secondary shear zone. (c) Chip separation and successive shearing of chip material entering the shear zone. (d) Final stages of the cutting process

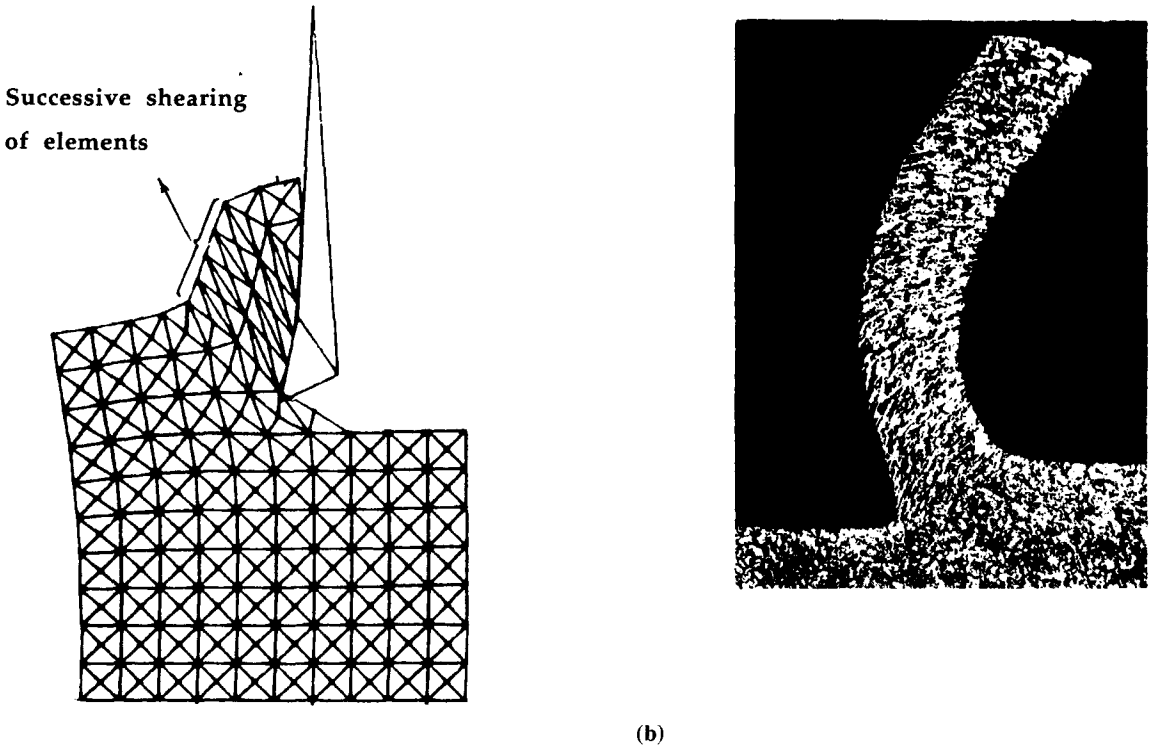

Fig. 12 Comparison of finite element simulation and experimental observation of the chip formation process. (a) Code results. (b) Experimental results (Ref 17)

to brittle fracture of chips. The simulation results for the prediction of the general chip geometry agreed well with the experimental results. However, a more realistic simulation requires utilization of significantly denser mesh, as well as a more complete constitutive equation that includes the effects of strain, strain rate hardening, and thermal softening.

An important phenomenon associated with the generation of segmental chips in the cutting of some metals, such as tita-

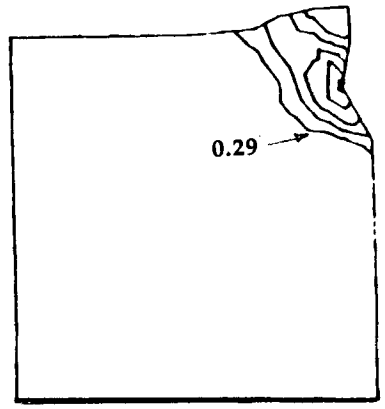

(a)

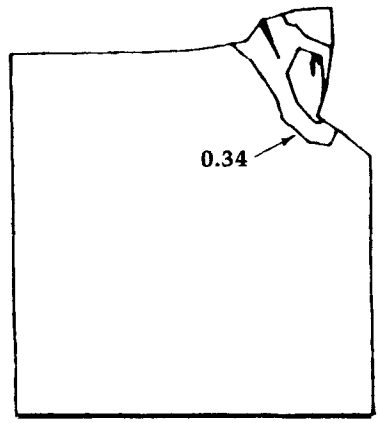

(b)

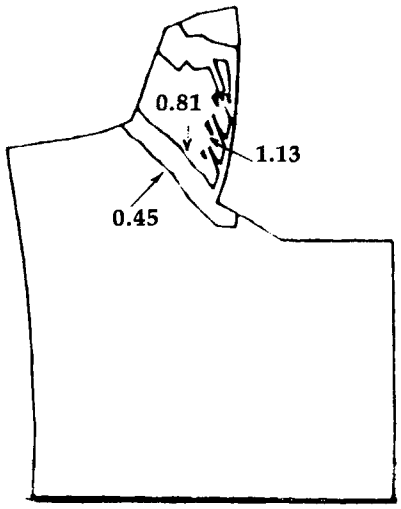

(c)

Fig. 13 Effective plastic strain contours at different cutting stages. (a) Initial chip compression stage. (b) Chip separation stage. (c) The steady-state cutting stage showing the location of both the primary and secondary shear zones

nium, is the formation of adiabatic shear bands along the shear plane. In order to perform realistic simulations of the cutting processes of those metals, the method presented in this paper, together with the utilization of highly fine mesh and a proper constitutive equation such as the one mentioned above, should prove necessary and effective.

Acknowledgments

This study was partially supported by a grant from the Advanced Technology Center of Southeast Pennsylvania through the Ben Franklin Partnership Program. The supercomputing time was furnished by a grant from the National Science Foundation through Pittsburgh Supercomputing Center. The authors are grateful to Dr. William Flis for valuable discussions.

References

1. M.C. Shaw, *Metal Cutting Principles*, Oxford Series on Advanced Manufacturing, 1984
2. I. Time, *Resistance of Metals and Woods to Cutting*, St. Petersburg, 1870
3. H. Tresca, Writings on the Machining of Metals, *Bull. Soc. d'Encouragement pour l'Industrie Nationale*, 1873, p 585-685
4. F.W. Taylor, On the Art of Cutting Metals, *Trans. ASME*, Vol 28, p 31-38
5. V. Piispanen, Theory of Formation of Metal Chips, *J. Appl. Phys.*, Vol 19, 1948, p 876-881
6. H. Ernst and M.E. Merchant, Chip Formation, Friction, and High-Quality Machined Surfaces, *Surface Treatment of Metals*, American Society for Metals, Vol 29, 1941, p 299
7. E.H. Lee and B.W. Shaffer, The Theory of Plasticity Applied to a Problem of Machining, *J. Appl. Mech.*, Vol 18, 1951, p 405-413
8. B.E. Klamecki, Incipient Chip Formation in Metal Cutting Processes—A Three Dimensional Finite Element Analysis, *J. Eng. Mater. Technol.*, Vol 106, 1984, p 132-138
9. E. Usui and T. Shirakashi, Mechanics of Machining: From Descriptive to Predictive Theory, *The Art of Cutting Metals—75 Years Later*, American Society of Mechanical Engineers, Vol 7, 1982, p 13-35
10. K. Iwata, K. Osakada, and Y. Terasaka, Process Modelling of Orthogonal Cutting by Rigid-Plastic Finite Element Method, *J. Eng. Mater. Technol.*, Vol 106, 1984, p 132-138
11. J.S. Strenkowski and J.T. Carrol, A Finite Element Model of Orthogonal Metal Cutting, *J. Eng. Industry*, Vol 107, 1983, p 349-354
12. J.T. Carrol and J.S. Strenkowski, Finite Element Models of Orthogonal Metal Cutting with Application to Single Point Diamond Turning, *Int. J. Mech. Sci.*, Vol 30 (No. 12), 1988, p 899-920
13. K. Komvopoulos and S.A. Erpenbeck, Finite Element Modelling of Orthogonal Metal Cutting, *J. Eng. Industry*, Vol 113, 1991, p 253-267
14. P.C. Chou and L. Wu, A Dynamic Relaxation Finite Element Method for Metal Forming Processes, *Int. J. Mech. Sci.*, Vol 28, 1986, p 231-250
15. P.C. Chou, J. Hashemi, A. Chou, and H. Rogers, Experimental and Computer Simulation of Shear Bands in Controlled Penetration Impacts, *J. Impact Eng.*, Vol 11 (No. 3), 1991, p 305-321
16. J. Hashemi, "Finite Element Simulation of Segmented Chip Formation in High-Speed Machining Process," Ph.D. thesis, Drexel University, 1988
17. K.H. Moltrecht, Machine Shop Practice, Industrial Press Inc., 1981.